Facile self-assembly synthesis of γ-Fe2O3 /graphene oxide for enhanced photo-Fenton reaction

Feifei Wang[a,b], S Yu, M Ge, Sujun Wu[a,b*], Juan Guan[a,b], Junwang Tang[c], Xiao Wu[d], Robert O. Ritchie[b,e]

[a] School of Materials Science and Engineering, Beihang University, Beijing 100191, China

[b] Intl. Research Centre for Advanced Structural and Biomaterials, Beihang University, Beijing 100191, China

[c] Solar Energy & Advanced Materials Research Group, Department of Chemical Engineering, University College London, London WC1E 7JE, U.K.

[d] Institute of Chemistry, Chinese Academy of Sciences, Beijing 100190, China

[e] Department of Materials Science & Engineering, University of California, Berkeley, CA 94720, USA

## Abstract

A novel self-assembly method was developed to prepare a $\gamma$-Fe$_2$O$_3$/graphene oxide (GO) composite catalyst which shows excellent synergy between photocatalysis and Fenton reactions. The $\gamma$-Fe$_2$O$_3$/GO composite prepared on the iron plates represents very efficient and reproducible photocatalystic activity for water treatment, e.g. 80 min to complete degradation of methylene blue (MB, 50 mg/L) as evidenced by the mineralized product sulphate ions, which is the non-biodegradable dye wastewater that is widely used in the textile industry. The composite catalyst has been proven to be stable over a wide pH range (from 2.0 to 11.9) for degradation of MB. It can be easily extracted from solution with a magnet and repeatedly used without loss of catalytic activity. The high activity and stability of the catalyst system is attributed to a synergistic interaction between $\gamma$-Fe$_2$O$_3$ and GO that facilitates charge separation, thereby accelerating Fenton processes and photocatalysis. In addition, the dominant reactive oxygen species responsible for the degradation of MB, *i.e.* the hydroxyl radical (•OH), which is generated by activation of H$_2$O$_2$ on the surface of the $\gamma$-Fe$_2$O$_3$/GO

---

*Corresponding author. tel: +86 1082316326; fax: +86 1082317108.
E-mail: wusj@buaa.edu.cn

composite, could be detected by a free-radical quenching experiment. A possible degradation mechanism is proposed that the adsorbed MB molecules are attacked by dominant responsible radicals of •OH on the surface of the $\gamma$-Fe$_2$O$_3$/GO composite. These beneficial characteristics of the $\gamma$-Fe$_2$O$_3$/GO composite to act as a catalyst could potentially provide a solution to resolve important environmental problems, especially dye wastewater treatment.

**Keywords:** Photocatalysis, Fenton reaction, self-assembly, graphene oxide, methylene blue degradation

# 1. Introduction

One of the adverse consequences of the modern industrialization is severe environmental pollution, the efficient and more importantly green technologies are thus urgent to remove these pollutants. One typical pollutant is colorful dyes which from various industries such as textiles, printing, food, paper, leather and cosmetics has become a serious environmental problem due to its high toxicity and slow self-degradation under natural conditions [1,2]. Some organic dyes and their products have detrimental mutagenic or carcinogenic effect on flora or fauna [3]. Developing a facile and efficient process to eliminate these dye pollutants has become increasingly important, in terms of benefitting the environment and human health [4]. Methods such as adsorption and flocculation have been used to remove the dye pollutants from wastewater [5,6] although many such treatment methods do not clean the pollutants completely and can produce secondary waste products which require further processing [7]. Chemical oxidation, or the conventional Fenton processes, is one of the most efficient, low cost and convenient advanced oxidation processes (AOPs) for water purification and wastewater treatment [8]. Nevertheless, strict reaction conditions such as highly acidic conditions (pH<4) and the generations of substantial iron sludge and waste catalyst remain a challenge [9].

Recently, an iron-based solid catalyst termed heterogeneous Fenton oxidative has afforded a promising alternative [10]. Iron and iron oxides have been widely used as heterogeneous Fenton catalysts because of their inexpensive, safe and environmental

friendly properties [11]; in particular, iron-based catalytic materials, such as $Fe_2O_3$, $Fe_3O_4$ and FeOOH have been well studied [12-14].

To improve the catalytic activity and stability of these iron-based heterogeneous Fenton catalysts, various supports such as Nafion, resin, zeolite, clays and carbon, have been studied [15-19]. In this regard, graphene oxide (GO) has attracted considerable attention as one of the supports because of its ordered nanometer to micrometer scale structure, its large surface area to volume and its high ratio of lateral size to thickness. Furthermore, GO provides high accessibility of reactants towards its active sites to diminish limitations in mass transfer during catalysis, and the oxygenated functional groups may act to immobilize iron oxide [20,21]. Various GO or reduced graphene oxide (RGO) supports have been reported. For example, RGO/FeOOH or $GO/Fe_2O_3$ has been shown to provide high catalytic activity over a wide pH range [22,23]; moreover, fabricated $RGO/Fe_3O_4$ or $GO/Fe_3O_4$ displays high and stable Photo-Fenton activity [24,25]. In these heterogeneous Fenton catalyst systems, the main active species is a hydroxyl radical ($\cdot OH$) on the catalyst surface; the transition between the metal ions and GO serve to enhance the formation of $\cdot OH$ through a strong synergistic interaction between both components [26,27].

Recently, progress has been made in preparing GO supported heterogeneous Fenton catalysts via various pathways, including by hydrothermal methods, co-precipitation methods, vacuum filtration or electrochemical methods [28-30]. However, the complexity and protracted nature of these techniques severely limit their scalability in synthesizing target products [31]. For example, Zubir *et al.* [20] prepared $GO/Fe_3O_4$ using a method which requires pre-hydrolyzing the ferric ions with alkali followed by drying of the black $GO/Fe_3O_4$ precipitates for 48h. Liu *et al.* [32] fabricated $GO/\alpha$-$Fe_2O_3$ by   stirring for 12h to hydrolyze a mixture of ferric nitrate, urea and GO. An alternative procedure was used by Liu *et al.* [33] to process poly (N-isopropylacrylamide)-GO membranes by vacuum filtration which could realize gradual small/medium/large molecule separation for water purification, but the preparation of this membrane again required a complex pre-treatment process, e.g., blending of N-isopropylacrylamide and GO.

Accordingly, we reasoned that there was significant utility to explore a facile way of preparing heterogeneous Fenton catalysts specifically from the perspective of improving efficiency and saving time. Consequently, in this study, a magnetically separable $\gamma$-Fe$_2$O$_3$/GO composite was synthesized by a simple self-assembly method, based on a technique first reported by Cao $et$ $al.$ to make functional thin films [34]. To confirm the universality of this self-assembly method for preparing heterogeneous catalysts, a series of the MO$_x$/GO (M=Zn, Cu, Co) composites was prepared by using different metal substrates. Compared to existing methods [35-37], this self-assembly method exhibits scalability, facile tunability and high efficiency. In the process of catalysis, methylene blue (MB) was chosen as a model cationic dye, as it is widely used in the industry [32] and represents a class of non-biodegradable dye wastewater which can cause serious damage to health if inhaled or ingested. The efficiency of the MO$_x$/GO composites for the MB degradation is studied and the related photodegradation and mineralization mechanisms discussed.

## 2. Experimental

### 2.1. Reagents and materials

Graphite powder (99.998 wt%, 200mesh) was purchased from Alfa Aecar Ltd. (Shanghai, China). Potassium permanganate (KMnO$_4$, 99.5 wt%), hydrogen peroxide (H$_2$O$_2$, 30 wt%), methanol (CH$_3$OH, 99.9 wt%) and sulfuric acid (H$_2$SO$_4$, 98 wt%) were obtained from Beijing Chemical Works (Beijing, China). Pure metal (99.9 wt%) plates (10$\times$10$\times$5 mm), including Iron, zinc, copper and cobalt plates, were purchased from Anyang Iron & Steel Group Co Ltd. Methylene blue (MB, 99.5 wt%) with a molecular formula C$_{16}$H$_{18}$ClN$_3$S$\cdot$3H$_2$O, p-Benzoquinone (BQ, 99 wt%) and terephthalic acid (TA, 99 wt%) used in this study were obtained from Aladdin Chemical Ltd (Shanghai, China). All chemicals were of analytical grade and used without further purification. Deionized (DI) water was utilized throughout the synthesis process.

### 2.2. Fabrication of the $\gamma$-Fe$_2$O$_3$/GO composite

Graphene oxide (GO) was prepared from graphite powder using a modified Hummers method [38]. Plates of iron substrate were mechanically polished by a series

of silicon carbide papers followed by polishing with alumina compounds. Once their surface roughness became less than 1 μm, the plates were ultrasonically cleaned in acetone, alcohol and deionized water in sequence for 15 min. The iron plates were then immersed in the GO solution at 40°C and the γ-Fe$_2$O$_3$/GO films were gradually formed on the surface of the iron. After 2 h, the iron plates together with the γ-Fe$_2$O$_3$/GO films were taken out of the solution and then oven dried at 60°C for 2 h. Following such processing, the γ-Fe$_2$O$_3$/GO films could be readily peeled from the iron substrate before being cut into small pieces for catalytic evaluation. Also, the MO$_x$/GO (M=Zn, Cu, Co) composites were prepared using the same method with zinc, copper and cobalt plates, respectively, as the substrate.

*2.3. Characterization*

Surface characteristics and the thickness of the prepared GO were evaluated with atomic force microscopy (AFM, Bruker, Dimension). The crystal structure of γ-Fe$_2$O$_3$/GO composite was characterized by x-ray diffraction (XRD, Rigaku, D/Max-2500) using Cu Kα radiation (λ=1.54184 Å) at room temperature. Surface morphology was observed by scanning electron microscope (SEM, TESCAN VEGA3), whereas the transmission electron microscope (TEM, Jeol, JSM 2100F) was used to analyze the nano-scale morphology of the catalyst. An investigation of surface components of the catalyst was carried out on x-ray photoelectron spectroscope (XPS, Thermo Scientific, Escalab 250Xi) using Al Kα monochromatized radiation. A Fourier transform infrared spectrometer (FTIR, Bruker, Tensor-27) equipped with a diamond ATR attachment was utilized to record FTIR spectra at room temperature in the range of 4000-550 cm$^{-1}$ with a 4 cm$^{-1}$ resolution over 32 scans. Raman spectra were obtained by employing a Raman spectrometer (Jobin Yvon, LabRAM HR800) with an excitation wavelength of 633 nm. The Brunauer-Emmett-Teller specific surface area (S$_{BET}$) of γ-Fe$_2$O$_3$/GO composite was characterized by nitrogen adsorption at 77 K with a Micromeritics 2020 instrument. Ultraviolet–visible (UV-vis) spectra were recorded on a UV-vis spectrometer (Metash, UV9000). UV–visible diffuse reflectance spectra were acquired using a spectrophotometer (UV–vis DRS, UV-3600, Shimadzu) with BaSO$_4$ used as the reference. Photoluminescence (PL) spectra of the catalyst was also measured at room

temperature using fluorescence spectrophotometer (Hitachi F-4500, Japan) with an excitation wavelength of 325 nm. The magnetization curve of the composite was measured with a vibrating sample magnetometer (VSM, Lake Shore, 7407). Thermogravimetric analysis (TGA) was carried out for the catalysts using a thermogravimetric analyzer (Netzsch, STA449F3) with a heating rate of 10°C/min in the air. Ion chromatography (Dionex, ICS-2100) and inductively coupled plasma optical emission spectroscopy (ICP-OES, Perkin Elmer, Optima 5300DV) were used to analyze the sulfate radical and iron ion content after catalytic testing, respectively.

## 2.4. Test of photocatalytic activity

The photocatalytic activities of the as-prepared catalyst were evaluated by photocatalytic degradation in MB aqueous solution under UV-vis light. A 500W high pressure Hg lamp was located 150 mm above the center of the solution as the UV-vis irradiation source. 10 mg of catalysts was added to the 50 ml MB solution (50 mg/L). Prior to irradiation, the catalytic systems without $H_2O_2$ were stirred in the dark for 30 min to establish adsorption-desorption equilibrium. Subsequently, the heterogeneous Fenton reaction was started when the lamp was turned on and 10 ml of $H_2O_2$ was added. About 2 ml solution was withdrawn at given time intervals and the catalysts collected by magnetic separation. The UV-vis absorbance of the MB solution was measured on UV-vis spectroscopy at 664 nm.

## 2.5. Measurement of radical formation

To explore the mechanisms involved in the catalytic degradation of MB in the $\gamma$-$Fe_2O_3$/RGO+$H_2O_2$+UV system, hydroxyl radicals and superoxide anion radicals were measured quantitatively. In the quenching experiment, methanol (MeOH) and benzoquinone (BQ) were added to this catalytic system as obligate •OH and $O_2$•$^-$ scavengers, respectively [32]. In addition, the generation of •OH was detected by using photoluminescence spectra (PL spectra). Typically, 10 mg of catalysts was dispersed in 50 ml of aqueous solution together with $5\times10^{-4}$ mol/L of terephthalic acid (TA) and $2\times10^{-3}$ mol/L of NaOH. 10 ml of 30% $H_2O_2$ was added and the lamp was turned on when TA had completely dissolved. After different time intervals, the concentration of

formed 2-hydroxyterephthalic in the solution was characterized using photoluminescence spectra.

## 3. Results and Discussion

### 3.1 Composition and structural characterizations

Fig. 1a presents the XRD patterns of the graphite, GO and $\gamma$-$Fe_2O_3$/GO composite. In this figure, there is a typical strong peak at $2\theta=26.9^o$ in the graphite curve, with the peak disappearing when the graphite was oxidized to GO. At this stage, a strong peak at $2\theta=10.6^o$ appeared ( shown in Fig. 1a as GO), which confirmed that graphite has successfully been converted to GO with a larger layer spacing of 0.8 nm [39]. The thickness of the GO was also examined using AFM and found to be approximately 1.4 nm (as shown in Fig.S1 in the Supplementary Information). The XRD patterns of as-prepared $\gamma$-$Fe_2O_3$/GO composite are shown as the $\gamma$-$Fe_2O_3$/GO curve in Fig.1a. The peaks at $2\theta=30.5^o$, $35.8^o$, $43.5^o$, $53.8^o$, $57.4^o$ and $63.0^o$ are respectively indexed as the (220), (311), (400), (422), (511) and (440) crystal planes of $\gamma$-$Fe_2O_3$ (JCPDS 25-1402). An XRD peak for the GO was not detected in the $\gamma$-$Fe_2O_3$/GO composite, probably because the intercalation of $\gamma$-$Fe_2O_3$ nanoparticles in GO limited the restacking of GO layers [40].

Raman spectroscopy was used to verify the co-existence of $\gamma$-$Fe_2O_3$ and GO in the $\gamma$-$Fe_2O_3$/GO composite. Fig.1 b shows two typical peaks at 1336 $cm^{-1}$(the D band represents disorder carbon) and at 1599 $cm^{-1}$(the G band represents graphitic carbon). The intensity ratio of these two bands ($I_D/I_G$) can be used to define the degree of structural defects and disorder in carbon materials [41]. This ratio in the $\gamma$-$Fe_2O_3$/GO composite ($I_D/I_G$=1.5) was larger than in the GO where $I_D/I_G$=1.09 [42], which indicates an increase in disorder for the $\gamma$-$Fe_2O_3$/GO composite and also confirms that the GO has become partially reduced due to the presence of iron. To further substantiate the formation of the $\gamma$-$Fe_2O_3$/GO composite, the low wave number region (400 $cm^{-1}$ to 1000 $cm^{-1}$) was fine scanned; in the inset to Fig. 1b, it can be seen that the two broad bands at 495 and 700 $cm^{-1}$ belong to $\gamma$-$Fe_2O_3$. Moreover, these two bands were not present in any other spectra of iron oxide and the oxyhydroxide [43].

The thermal stability and thermal decomposition behavior of the synthetic composite were studied using the TGA technique. Fig. 1c shows three steps associated with weight loss as a function of temperature below 150°C, 205-296°C and 331-490°C in the $\gamma$-$Fe_2O_3$/GO composite under an air atmosphere [44]. The weight loss below 150°C was attributed to dehydration of physically adsorbed water. During the second step around 200°C, the weight loss was probably due to the decomposition of oxygen-containing groups on the surfaces of the GO. The decomposition of the GO was the fastest at 257°C, although it slowed down at temperature from 257°C to 296°C due to the reduction in the oxygen-containing groups (see the DTG curve in Fig.1c). The third step from 331°C to 490°C was associated with the removal of the carbon skeleton because of the burning of the GO; the decomposition of the carbon skeleton at 420°C was the fastest but it also slowed down with increase in temperature. Above 500°C, the weight loss rate (derivative weight) was close to zero, indicating that the carbon skeleton was almost completely burnt out. At temperatures between 730°C and 800°C, the weight percent was constant at a value of 84% which can be considered as the $Fe_2O_3$ content. Therefore, the mass percentage of $\gamma$-$Fe_2O_3$ in the $\gamma$-$Fe_2O_3$/GO composite is estimated to be 84% from this self-assembly method.

**Fig. 1**: (a) XRD patterns of graphite, GO and $\gamma$-Fe$_2$O$_3$/GO composite, (b) Raman spectra of GO and the $\gamma$-Fe$_2$O$_3$/GO composite, (c) TG and DTG curves of the $\gamma$-Fe$_2$O$_3$/GO composite.

The surface chemical compositions and electronic state of the $\gamma$-Fe$_2$O$_3$/GO composite were analyzed by XPS. The survey spectra (Fig. 2a) show the presence of the Fe 2p, O1s and C1s energy regions. The high-resolution Fe 2p spectrum in Fig. 2b shows the two peaks at 710.5 eV and 724.1 eV of the binding energy of Fe 2p that correspond to Fe 2p$_{3/2}$ and Fe 2p$_{1/2}$, respectively. The doublet peaks of iron element indicate different redox status of surface $\gamma$-Fe$_2$O$_3$. The O 1s spectrum (Fig. 2c) can be deconvoluted into three different peaks at 529.3 eV, 530.7 eV and 532.1 eV. The peaks at 529.3 eV can be assigned to oxygen binding with Fe (Fe-O) [45]. The peak with binding energy of 530.7 eV can be assigned to the lattice hydroxyl with Fe (denote as Fe-OH). Finally, the peak at 532.1 eV is deduced to be oxygen containing groups bonded with C atoms in GO (C-OH/C-O-C) [32]. Fig. 2d shows the C 1s spectrum that can be deconvoluted into four different peaks, indicating the C-C/C=C bonds (284.1 eV), the C-O bonds (epoxy and hydroxyl) at 286.2 eV, the C=O at O-C-O bonds (287.1 eV), and the O-C=O (carboxylate) bonds at 288.4 eV [46].

The vibration mode of functional groups in GO or the $\gamma$-Fe$_2$O$_3$/GO composite were analyzed by FTIR spectra (shown in Fig. S2). The C=O stretch vibration (1726 cm$^{-1}$), -OH bend vibration and C=C stretch vibration (1613 cm$^{-1}$), the C-OH bend vibration (1432 cm$^{-1}$), and the C-O stretch vibration of epoxy or alkoxy (1044 cm$^{-1}$) are all observed in the GO curve [28]. A broad band around 3331 cm$^{-1}$ of the -OH stretch vibration of GO is also found [47]. In addition, other weaker peaks, such as the C-O functional groups of GO, are also observed in the FTIR spectra of the $\gamma$-Fe$_2$O$_3$/GO composite, indicating that the $\gamma$-Fe$_2$O$_3$ nanoparticles are anchored on the GO sheets. More importantly, the spectra of the $\gamma$-Fe$_2$O$_3$/GO composite before and after MB degradation appear to be almost the same, which strongly implies the excellent stability of the $\gamma$-Fe$_2$O$_3$/GO composite.
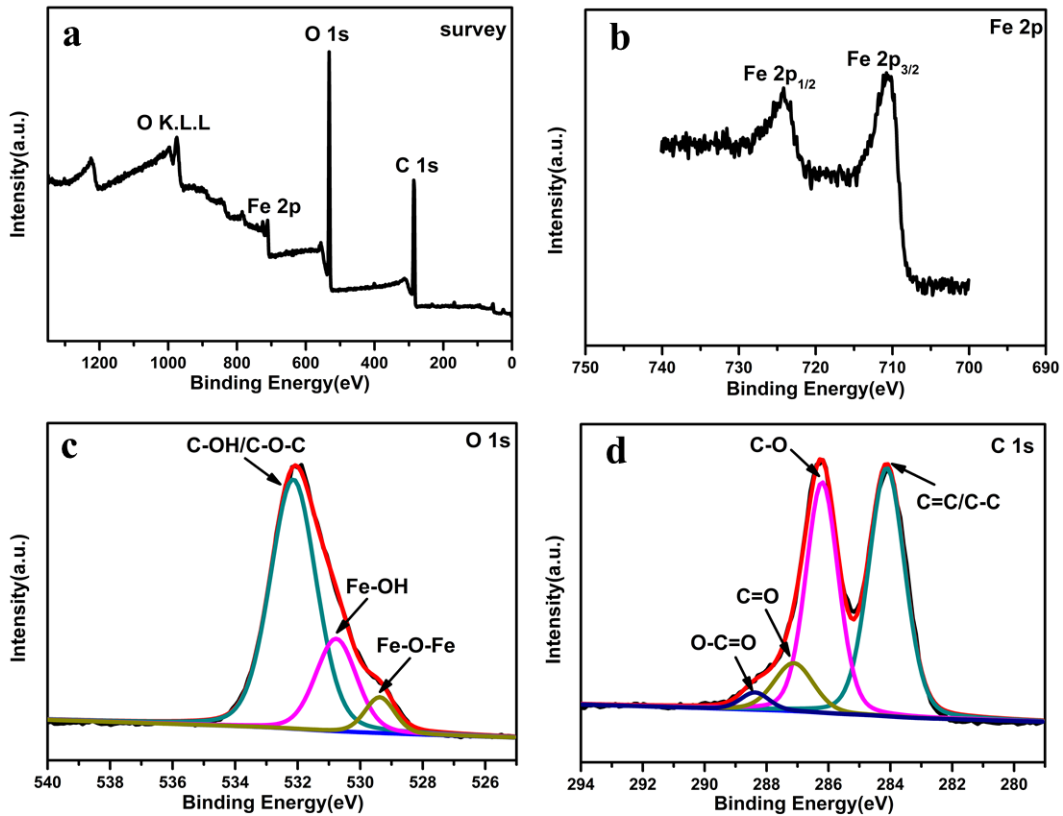
**Fig. 2:** XPS spectra of the γ-Fe₂O₃/GO composite: (a) survey scan, (b), (c) and (d) are high-resolution spectra of the Fe 2p, O 1s and C 1s, respectively.

The surface and cross-section morphology of the γ-Fe₂O₃/GO composite are shown in Fig. 3a and b, respectively. The γ-Fe₂O₃/GO composite has a wrinkled surface due to the rippled shape of the GO sheets, as shown in Fig. 3a. The thickness of the composite is about 1.2 μm (Fig. 3b). The digital photo inset in Fig. 3b reveals its flake-like macroscopic morphology. This figure also suggests that the GO with iron oxides is assembled into a lamellar structure on the iron plates. Moreover, the thickness and the area of the γ-Fe₂O₃/GO composite could be controlled by volume of GO solution and its concentration. The presence of dense, sphere-like γ-Fe₂O₃ nanoparticles anchored on the surface of the GO is clearly apparent in the TEM images in Fig. 3c. The γ-Fe₂O₃ is well dispersed on the surface of the GO sheets, which can act to hinder aggregation and provide channels to promote mass transport [48]. The structure of GO sheets supported γ-Fe₂O₃ nanoparticles could produce a synergistic effect through providing efficient charge/mass transfer between γ-Fe₂O₃ nanoparticles and GO sheets and thereby accelerating Fenton processes and photocatalysis.
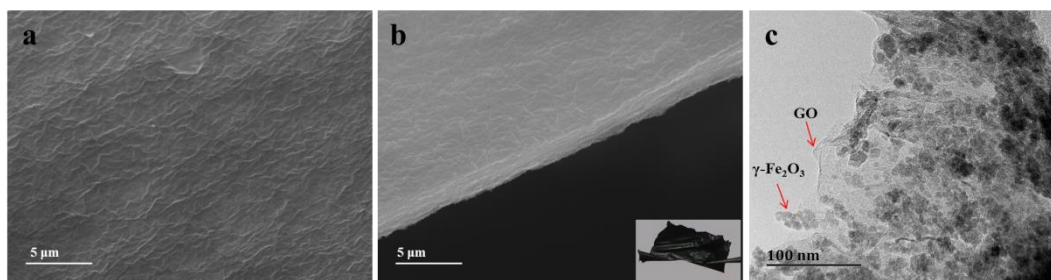
**Fig. 3:** SEM images of (a) the surface and (b) the cross-section of the γ-Fe$_2$O$_3$/GO composite; (c) TEM image of the γ-Fe$_2$O$_3$/GO composite.

### 3.2. Fenton catalytic activity measurements

The Fenton catalytic activity of the γ-Fe$_2$O$_3$/GO composite was studied for its effect on the degradation of the MB assisted by UV light. Unlike traditional powder catalysts, the prepared lamellar structure of γ-Fe$_2$O$_3$/GO catalyst was directly put into MB solution, which can easily be retrieved back for recycling. Fig. 4a shows two typical main peaks (614 nm and 665 nm) of MB spectra in the 8th cycle; the absorption peak is attributed to the chromophores groups (-C=S and –C=N) in the MB molecular. The two peaks decreased with increasing time, and the solution gradually turned colorless within 60 min (shown in the inset of Fig. 4a). The dramatic decrease of the peak at 665nm indicates the destruction of the conjugate structure in the MB molecules.

Fig. 4b shows the degree of decolorization of the MB under different conditions. The decolorization of MB using UV photolysis alone could reach 11% (black data). With the addition of H$_2$O$_2$ and incident UV irradiation, the degree of decolorization of the MB increased to 36% (red data), which could be attributed to the small amount of •OH generated by H$_2$O$_2$ under UV irradiation and promoted by the decomposition of chromophores in the MB molecules [32]. However, a similar low degree of decolorization appeared in the γ-Fe$_2$O$_3$+UV+H$_2$O$_2$ systems (blue data), which indicates that the added γ-Fe$_2$O$_3$ nanoparticles alone could not promote the degradation of the MB molecules, because the agglomeration of the γ-Fe$_2$O$_3$ nanoparticles would leach only a few effective catalytic Fe$^{2+}$ components. It is worth noting here that the degree of decolorization of the MB reached 99% within 80 min in the γ-Fe$_2$O$_3$/GO +UV+H$_2$O$_2$ systems (green data), while the degree of decolorization of MB with γ-Fe$_2$O$_3$/GO in the dark (pink data) was only 25% after 120 min. Apparently, GO acts as supports that can

exert positive synergistic effects under UV irradiation, which are related to mechanical interactions and chemical binding between γ-Fe$_2$O$_3$ and GO. On the one hand, the γ-Fe$_2$O$_3$ nanoparticles were uniformly dispersed on the GO sheets to avoid agglomeration (as shown in Fig.3c), on the other hand, the formation of Fe-O-H bonds could enhance the chemical interaction between γ-Fe$_2$O$_3$ and GO to facilitate the high catalytic efficiency of MB and suppress the iron ion leaching [45]. Moreover, the Brunauer-Emmett-Teller (BET) specific surface area ($S_{BET}$) of the γ-Fe$_2$O$_3$/GO composite was calculated to be 88.01 m$^2$/g (as shown in Fig. S3a); further, the pore size distribution shows a sharp maximum at approximately 3.8 nm due to the existence of the mesoporous structure in the composite (as shown in Fig. S3b). These mesoporous structures might provide more absorption or reaction sites to increase catalytic activity in the degradation process [41].
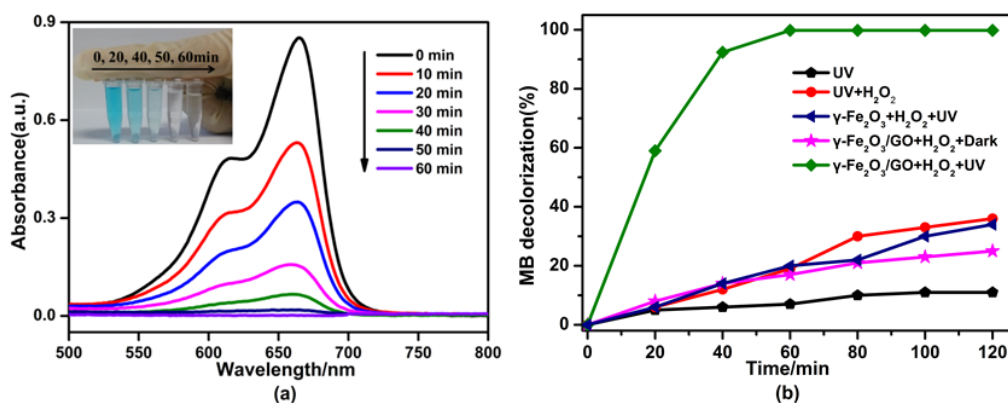


**Fig. 4:** (a) UV–vis spectra during decolorization of MB in the γ-Fe$_2$O$_3$/GO + H$_2$O$_2$+ UV system and (b) the decolorization of the MB under different conditions.

The optical absorption properties of the γ-Fe$_2$O$_3$/GO catalyst were investigated by UV-vis diffuse reflectance spectra. As can be seen from Fig. 5a, the γ-Fe$_2$O$_3$/GO catalyst exhibits strong absorption over a wide wavelength range of 200 to 800 nm, suggesting that the catalyst can absorb a wide range of light and improve its catalytic activity under photo-irradiation. In addition, the catalytic activity of the MO$_x$/GO (M=Zn, Cu, Co) composites were evaluated. As seen from Fig. 5b, the CuO$_x$/GO and CoO$_x$/GO composites needed 60 min to reach 99% MB decolorization (pink and red data, respectively), while the ZnO$_x$/GO composite showed 47% MB decolorization after 120 min (blue data). All the three decolorization rates of the MO$_x$/GO heterogeneous

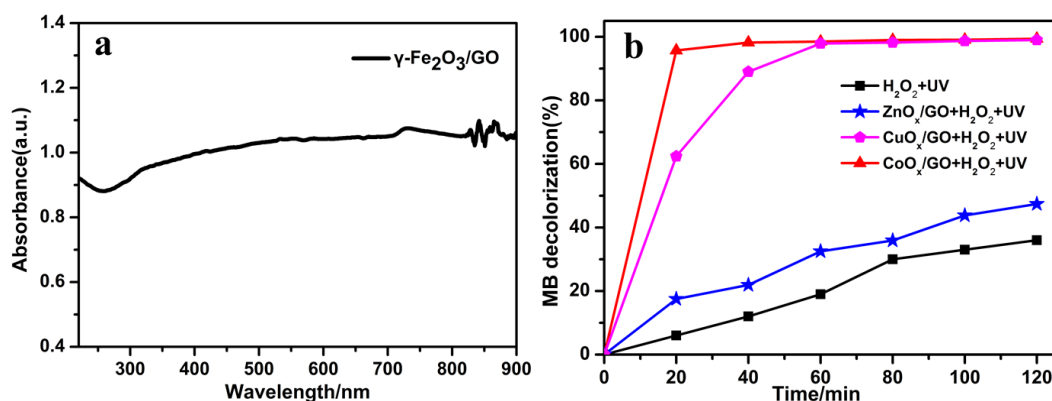catalysts are higher than that of the $H_2O_2$ +UV system (black data).



**Fig. 5:** (a) UV-vis diffuse reflectance spectra of the $\gamma$-Fe$_2$O$_3$/GO composite, and (b) the MB decolorization of composite prepared by different metal plates.

The stability at different acidic conditions and reusability of the $\gamma$-Fe$_2$O$_3$/GO heterogeneous Fenton catalyst are important factors for its practical application. The recyclability properties (Fig. 6a) were tested, and the catalytic activity of the $\gamma$-Fe$_2$O$_3$/GO composite was examined at different initial pHs from 2.0 to 11.9 (Fig. 6b). The MB decolorization ratio remained at near 99% after eight successive cycles, indicating its excellent stability and photo activity. It is worth noting that the catalytic completion time changed from 80 min to 60 min after the 8th cycle. This result can be attributed to an increase in the active sites because of the breakage of the catalysts into smaller pieces during the magnetic stirring process. More importantly, leaching of iron ion from the catalysts was not detected or was at a rate lower than the ion detection limit of ICP-OES in the repeated cycles. It is clear that the catalyst possesses excellent long term durability due to the strong interaction between $\gamma$-Fe$_2$O$_3$ and GO, and can be repeatedly used without any loss of catalytic activities. The results in Fig. 6b show that the catalytic activity of the $\gamma$-Fe$_2$O$_3$/GO catalyst remained almost the same in the pH range from 4.2 to 11.9 with a high degree of decolorization of 99% within 80min of reaction. This stability could be attributed to the electronegative surface of the GO which tends to adsorb cationic MB molecules by $\pi$-$\pi$ stacking and electrostatic interactions [32]. The time for complete decolorization was 100 min when the initial pH was 2.0. The slightly decreased decolorization rate may be ascribed to the formation of complex species $[Fe(H_2O)_6]^{2+}$ and stable oxonium ion $[H_3O_2]^+$ under conditions of high $H^+$ concentration, which act to ease the production of •OH. Yang *et al.* [49]

reported that the MB decolorization using the Fe/Fe$_3$O$_4$/GO composite was only 83% when the pH is 2. It can therefore be concluded that the γ-Fe$_2$O$_3$/GO catalyst owns great catalytic activity over a really wide range of pH and it could be used in a wide range of environmental conditions.

Apart from decolorization, the extent of MB mineralization is also important for industrial applications. The mineralization process is that an organic S-containing compound will become SO$_4^{2-}$ in MB solution. The SO$_4^{2-}$ concentration in solution can be determined by ion chromatography. The concentration of SO$_4^{2-}$ was 11.3 mg/L (0.5 mg/L SO$_4^{2-}$ from H$_2$O$_2$) after the 8$^{th}$ consecutive cycle, while the theoretical value is 12.8 mg/L. Therefore, the mineralization rate of solution reached 84% even after eight cycles, indicating the high catalytic activity and excellent reusability.
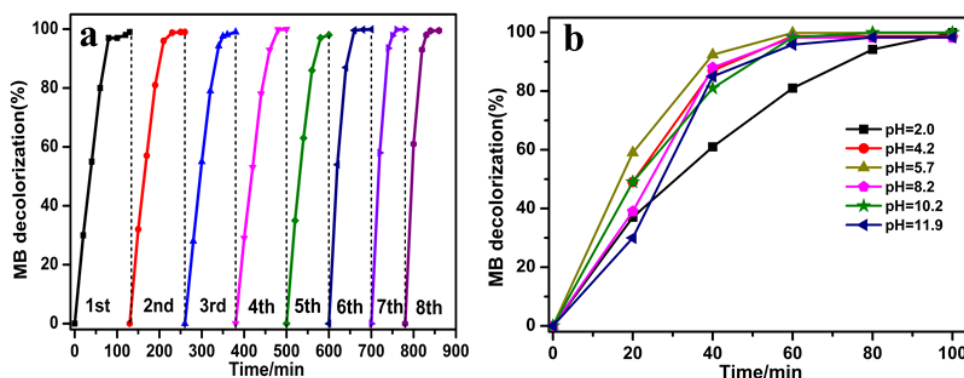


**Fig. 6:** (a) Repeated discoloration of MB solution of γ-Fe$_2$O$_3$/GO composite, and (b) discoloration of the MB at different initial pHs.

The magnetic properties of the as-prepared γ-Fe$_2$O$_3$/GO composite were tested by vibrating sample magnetometer (VSM) at room temperature. At the same time, the magnetic hysteresis of γ-Fe2O3 was also assessed in order to compare with the γ-Fe$_2$O$_3$/GO composite. As seen in Fig. 7, the γ-Fe$_2$O$_3$/GO composite shows super-paramagnetic behavior with nearly zero coercivity and nearly no remanence effect. The saturation magnetization (*Ms*) of the γ-Fe$_2$O$_3$/GO composite has a value of 40.9 emu·g$^{-1}$, which is lower than the γ-Fe$_2$O$_3$ composite (52.6 emu·g$^{-1}$), mainly due to the existence of the GO in the γ-Fe$_2$O$_3$/GO composite [4]. However, the γ-Fe$_2$O$_3$/GO composite can still be readily separated through an external magnetic field due to its large saturation magnetization (shown in the inset in Fig.7).
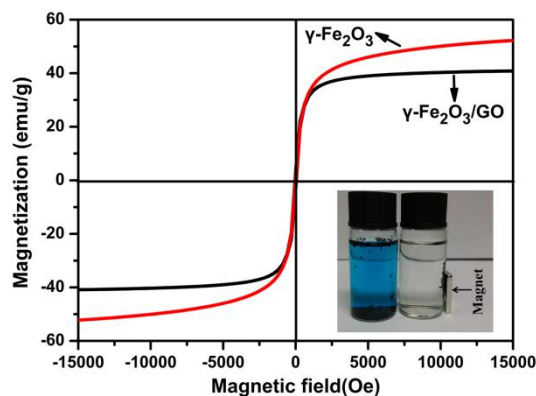
**Fig. 7:** Magnetic hysteresis curve of a γ-Fe$_2$O$_3$ nanoparticle and the γ-Fe$_2$O$_3$/GO composite.

Many studies have confirmed that the hydroxyl radical (•OH) and superoxide (O$_2$•$^-$) are the principal radicals detected using quenching experiments or electron spin resonance spectroscopy in photo-assisted iron oxide Fenton systems [50-52]. In this study, methanol (MeOH) and p-benzoquinone (BQ) were used as scavengers for •OH and O$_2$•$^-$, respectively. Fig. 8 shows the quenching effect on MB decolorization in the γ-Fe$_2$O$_3$/GO heterogeneous Fenton catalyst. It can be seen that MB decolorization is significantly suppressed in the presence of methanol, while adding BQ had a slight influence on MB decolorization, implying that •OH species are the dominant radicals during the decolorization process. To further confirm the generation of •OH, the Photoluminescence spectra (PL) technique using terephthalic acid (TA) as a probe molecule was utilized [53]. Fig.S4 shows the PL of γ-Fe$_2$O$_3$/GO+H$_2$O$_2$+UV systems in the presence of TA. A gradual increase in PL intensity with increasing time is observed, indicating that the amount of •OH generated by the system increased with time.

Based on the above mentioned experimental details and specific analysis, a schematic illustration of positive synergistic effect between the γ-Fe$_2$O$_3$ nanoparticles and GO sheets with the assistance of H$_2$O$_2$ and UV light is given in Fig. 9. Firstly, the MB molecule can be adsorbed on the surface of the GO sheets through electrostatic interactions and π-π stacking [32]. Then the GO sheets with a band gap of 2.79 eV and γ-Fe$_2$O$_3$ nanoparticles with a band gap of 2.30 eV can be activated to produce electrons and holes ($e$- and $h^+$) pairs in the conduction bands and valence bands, respectively [54,55]. The photo-generated electrons can spontaneously transfer from the γ-Fe$_2$O$_3$ conduction band to GO conduction band. The electrons are therefore efficiently

captured by $H_2O_2$ to form •OH radicals. Hydroxyl radicals have a strong oxidation potential and can thus oxidize MB into $CO_2$, $SO_4^{2-}$ and other inorganic substances [56]. Moreover, the photo-generated holes can directly oxidize MB. The charge separation and suppression of carrier recombination due to the synergistic interaction between γ-$Fe_2O_3$ and GO are realized, which can accelerate the Fenton process and photocatalysis. Therefore, the γ-$Fe_2O_3$/GO catalyst prepared by our self-assembly method appears to markedly enhance the degradation of the MB under UV irradiation though synergistic interactions between GO supports and the γ-$Fe_2O_3$ nanoparticles.
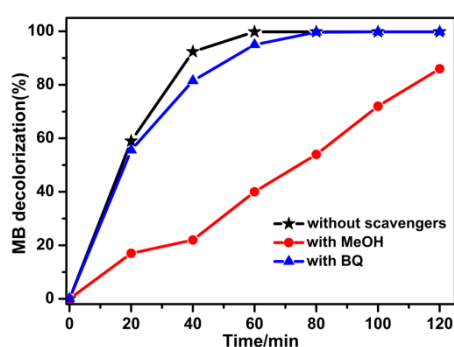


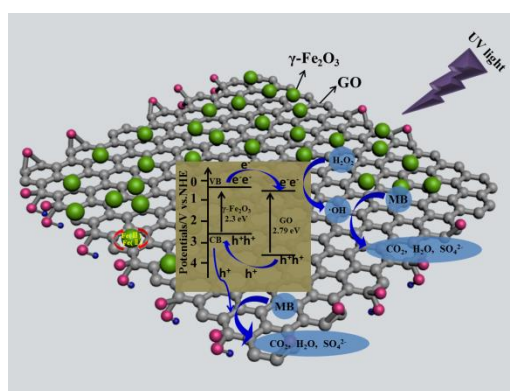**Fig. 8:** MB discoloration in presence of radical scavengers



**Fig. 9:** Schematic illustration of the proposed mechanism for MB degradation of γ-$Fe_2O_3$/GO catalyst under UV irradiation.

## 4. Conclusion

A novel and facile self-assembly method is demonstrated to successfully synthesize a γ-$Fe_2O_3$/GO heterogeneous Fenton catalyst on iron plates. The γ-$Fe_2O_3$/GO composite with 84 wt% γ-$Fe_2O_3$ nanoparticles dispersed on GO sheets exhibited good Fenton catalytic activity for the degradation of methylene blue (MB) with the assistance of UV irradiation. The MB degradation was completed within 80 min and the composite

catalyst was re-used for eight cycles with little loss of catalytic activities, demonstrating the potential of the catalyst to practical application in dye water treatment .Furthermore the catalyst could be effectively used over a wide range of pH (2.0-11.9), and readily separated from the purified water using a magnet. These excellent catalytic activities are attributed to the synergistic interactions between the GO supports and the $\gamma$-$Fe_2O_3$ nanoparticles. It is found that the charge separation at the $\gamma$-$Fe_2O_3$ and GO interface can suppress the carrier recombination, such that the •OH radicals formed through interaction between electron and $H_2O_2$ together with photo-generated holes both can oxidize MB. Therefore, the overall preparation, separation and re-use of the $\gamma$-$Fe_2O_3$/GO catalyst could reduce operating costs and increase degradation productivity, which may provide economic solutions to the environmental issues, especially to clean-up of dye wastewater pollutions.

# References

[1] M. Munoz, Z.M.D. Pedro, J.A. Casas, J.J. Rodriguez, Appl. Catal. B: Environ. 176–177 (2015) 249-265.

[2] T. Techalertmanee, S. Chancharoenrith, M. Namkajorn, S. Kiatisevi, L. Chaicharoenwimolkul, E. Somsook, Mater. Lett. 145 (2015) 224-228.

[3] T. Liu, Y. Li, Q. Du, J. Sun, Y. Jiao, G. Yang, Z. Wang, Y. Xia, W. Zhang, K. Wang, Colloids & Surfaces B Biointerfaces. 90 (2012) 197-203.

[4] X. Yang, W. Chen, J. Huang, Y. Zhou, Y. Zhu, C. Li, Sci. Rep. 5 (2015) 10632.

[5] X. Zhang, D. Liu, L. Yang, L. Zhou, T. You, J. Mater. Chem. A. 3 (2015) 10031-10037.

[6] Y. Dong, T. Wang, X. Wan, D. He, J. Geosci. Environ. Protect. 3 (2015) 66-71.

[7] A. Muthukrishnaraj, S. Vadivel, V.P. Kamalakannan, N. Balasubramanian, Mater. Res. Innov. 19 (2015) 258-264.

[8] L.M. Pastrana-Martínez, N. Pereira, L. Rui, J.L. Faria, H.T. Gomes, A.M.T. Silva, Chem. Eng. J. 261 (2015) 45-52.

[9] M. Triki, S. Contreras, F. Medina, J. Sol-Gel Sci. Technol. 71 (2014) 96-101.

[10] M. Munoz, Z.M.D. Pedro, J.A. Casas, J.J. Rodriguez, Appl. Catal. B: Environ. 176–177 (2015) 249-265.

[11] X. Wang, C. Liu, X. Li, F. Li, S. Zhou, J. Hazard. Mater. 153 (2008) 426-433.

[12] Z.M. Cui, Z. Chen, C.Y. Cao, L. Jiang, W.G. Song, Chem. Commun. 49 (2013) 2332-2334.

[13] T. Zeng, X. Zhang, S. Wang, Y. Ma, H. Niu, Y. Cai, Chemistry. 20 (2014) 6474-6481.

[14] R. Matta, K. Hanna, S. Chiron, Sci. Total Environ. 385 (2007) 242-251.

[15] A.L. Macedo, J.D. Fabris, M.J.M. Pires, W.L. Oliveira, J.D. Ardisson, R. Augusti, F.H. Aragón, R.S. Santos, L.C.A. Oliveira, M.C. Pereira, J. Braz. Chem. Soc. 27 (2016) 2290-2299.

[16] S. Guo, G. Zhang, J. Wang, J. Colloid Interf. Sci. 433 (2014) 1-8.

[17] X. Liu, Q. Zhang, B. Yu, R. Wu, J. Mai, R. Wang, L. Chen, S.T. Yang, Catalysts. 6 (2016) 146.

[18] S. Parra, L. Henao, E. Mielczarski, J. Mielczarski, P. Albers, E. Suvorova, J. Guindet, Langmuir. 20

(2004) 5621-5629.

[19] M. Cheng, W. Ma, J. Li, A. Yingping Huang, J. Zhao, Y.X. Wen, Y. Xu, Environ. Sci. Technol. 38 (2004) 1569-1575.

[20] N.A. Zubir, C. Yacou, J. Motuzas, X. Zhang, X.S. Zhao, D.D.C. Jc, Chem. Commun. 51 (2015) 9291-9293.

[21] N. Agarwal, R. Bhattacharyya, N.K. Tripathi, S. Kanojia, D. Roy, K. Mukhopadhyay, P.N. Eswara, PCCP. 19 (2017) 16329-16336.

[22] S. Guo, G. Zhang, Y. Guo, J.C. Yu, Carbon. 60 (2013) 437-444.

[23] Y. Wang, J. Fang, J.C. Crittenden, C. Shen, J. Hazard. Mater. 329 (2017) 321-329.

[24] B. Qiu, Q. Li, B. Shen, M. Xing, J. Zhang, Appl. Catal. B: Environ. 183 (2016) 216-223.

[25] L. Yu, J. Chen, Z. Liang, W. Xu, L. Chen, D. Ye, Sep. Purif. Technol. 171 (2016) 80-87.

[26] W. Z, W. J, Environ. Sci. Pollut. Res. 23 (2016) 18542-18551.

[27] N.A. Zubir, C. Yacou, J. Motuzas, X. Zhang, J.C.D.D. Costa, Sci. Rep. 4 (2014) 4594.

[28] M. Nawaz, W. Miran, J. Jang, D.S. Lee, Appl. Catal. B: Environ. 203 (2017) 85-95.

[29] Z. Wan, J. Wang, J. Hazard. Mater. 324 (2017) 653-664.

[30] H. Zhao, S. Chen, X. Quan, H. Yu, H. Zhao, Appl. Catal. B: Environ. 194 (2016) 134-140.

[31] J. Zhang, T. Yao, C. Guan, N. Zhang, H. Zhang, X. Zhang, J. Wu, J. Colloid Interf. Sci. 505 (2017) 130-138.

[32] Y. Liu, W. Jin, Y. Zhao, G. Zhang, W. Zhang, Appl. Catal. B: Environ. 206 (2017) 642-652.

[33] J. Liu, A. Karton, W. Li, W. Zhang, F. Guo, L. Hou, Q. Cheng, L. Jiang, D.A. Weitz, Y. Zhao, Nat. Commun. 8 (2017) 2011.

[34] X. Cao, D. Qi, S. Yin, J. Bu, F. Li, C.F. Goh, S. Zhang, X. Chen, Adv. Mater. 25 (2013) 2957-2962.

[35] S. Li, G. Zhang, W. Zhang, H. Zheng, W. Zhu, N. Sun, Y. Zheng, P. Wang, Chem. Eng. J. 326 (2017) 756-764.

[36] H. Maleki, Chem. Eng. J. 300 (2016) 98-118.

[37] Z.T. Hu, S.K. Lua, T.T. Lim, ACS Sustain. Chem. Eng. 3 (2015) 2726-2736.

[38] O.R.E. Jr William S H, J. Am. Chem. Soc. 80 (1958) 1339.

[39] P.F. Li, Y. Xu, X.H. Cheng, Surf. Coat. Technol. 232 (2013) 331-339.

[40] A.H. Mady, M.L. Baynosa, D. Tuma, J.J. Shim, Appl. Catal. B: Environ. 203 (2017) 416-427.

[41] A.H. Mady, M.L. Baynosa, D. Tuma, J.J. Shim, Appl. Catal. B: Environ. 203 (2017) 416-427.

[42] Y. Li, J. Qu, F. Gao, S. Lv, S. Lin, C. He, J. Sun, Appl. Catal. B: Environ. 162 (2015) 268-274.

[43] D.L.A.D. Faria, S.V. Silva, M.T.D. Oliveira, J. Raman Spectrosc. 28 (1997) 873–878.

[44] Z.T. Hu, S.K. Lua, T.T. Lim, ACS Sustain. Chem. Eng. 3 (2015) 2726-2736.

[45] X. Qian, R. Meng, Z. Yao, D. Yue, H. Yu, J. Jia, Y. Zhao, Environ. Sci. Technol. 51 (2017) 3993-4000.

[46] H. Moussa, E. Girot, K. Mozet, H. Alem, G. Medjahdi, R. Schneider, Appl. Catal. B: Environ. 185 (2016) 11-21.

[47] C. Wan, J. Li, ACS Sustain. Chem. Eng. 3 (2015) 2142-2152.

[48] Q. Zheng, Z. Cai, Z. Ma, S. Gong, Acs Appl. Mater. Interf. 7 (2015) 3263-3271.

[49] B. Yang, Z. Tian, L. Zhang, Y. Guo, S. Yan, J. Water Proc. Engin. 5 (2015) 101-111.

[50] C. Ruales-Lonfat, J.F. Barona, A. Sienkiewicz, M. Bensimon, J. Vélez-Colmenares, N. Benítez, C. Pulgarín, Appl. Catal. B: Environ. 166–167 (2015) 497-508.

[51] Y. Liu, X. Liu, Y. Zhao, D.D. Dionysiou, Appl. Catal. B: Environ. 213 (2017) 74-86.

[52] X. Qian, M. Ren, Y. Zhu, D. Yue, Y. Han, J. Jia, Y. Zhao, Environ. Sci. Technol. 51 (2017) 3993-4000.

[53] S. Guo, G. Zhang, J.C. Yu, J. Colloid Interf. Sci. 448 (2015) 460-466.

[54] D.B. And, R. Amal, G.K.C. Low, S. Mcevoy, J.phys.chem.b. 104 (2000) 4387-4396.

[55] I. Shown, H.C. Hsu, Y.C. Chang, C.H. Lin, P.K. Roy, A. Ganguly, C.H. Wang, J.K. Chang, C.I. Wu, L.C. Chen, Nano Lett. 14 (2014) 6097-6103.

[56] H. Chen, W. Liu, Z. Qin, Catalysis. Sci. Technol. 7 (2017).